Knowledge-based Segmentation: Using Simultaneous Shape Priori and Histogram Information to Segment Brain Structures

Nematollah Batmanghelich[1,2] , Hamid Soltanian-Zadeh[1,2,3], Babak Najaar Araabi[1,2]

[1]Control and Intelligent Processing Center of Excellence, Elec. and Comp. Eng. Dept., Faculty of Engineering, University of Tehran, Tehran, Iran
[2]School of Cognitive Sciences, Institute for Studies in Theoretical Physics and Mathematics, Tehran, Iran
[3]Image Analysis Lab. Radiology Dept., Henry Ford Health System, Detroit, Michigan, USA
E-mails: k.batman@ece.ut.ac.ir, {hszade,araabi}@ut.ac.ir

ABSTRACT
In this paper, we propose a new method integrating both *a priori* shape information and our knowledge about gray levels of the desired structure. We describe an approach inspired from tracking to deal with non-uniform gray levels. We define focus region to consider both interior and exterior of the desired object. We utilize signed distance function to consider shape information. Embedding *a priori* shape and gray level knowledge in a statistical platform, we use correlation between changes in shape and histogram to improve the results. Our method successfully segments Thalamus and other brain structures.

KEY WORDS
Brain Structural segmentation, Histogram information, Shape priori, Medical image analysis , Magnetic resonance imaging (MRI)

1. Introduction

Proposed by Osher et al [1], a category of geometric deformable models, also known as level set, has had enormous impact on medical image analysis in different areas ranging from segmentation to shape analysis. Although different kinds of deformable templates have been suggested so far (Kass et. al [2], Cootes et al [3], etc.), it is rare to see both topology preservation and fast shape recovery in a single platform. Level set methods may be categorized into two main classes: "level sets without regularizers" and "level sets with regularizers" (for a good survey, see the article by Suri et al [4]). Shape-based level set, first proposed by Leventon et al [5], is a level set with regularizer. They added a new term to the conventional level set partial differential equation to consider shape information. They estimated shape and pose parameters under maximum a posteriori probability framework (MAP). However, they did not consider gray level information of the desired structure. In addition, they tested their method for structures such as corpus callosum, which is easily distinguishable in sagittal brain in MRI. Furthermore, inasmuch as they used an edge-based approach, their method has the limitations of the edge-based methods. Tsai et al [6] and Yang et al [7] proposed mutual information-based and neighbor constrained level set methods based on Leventon's work.

We propose a new method inspired from tracking problems. We define a *focus* region to consider certain neighboring pixels outside the desired structure. Due to the imaging and anatomical impacts, there may be correlations between shape of the structure and its histogram. We consider correlations between structure histogram and shape. We evaluate our method on Thalamus, a challenging structures for segmentation, which has a key function in the sensory system [8]. Its specifications like volume and intensity in MRI are expected to change by certain neurological diseases [9]. We involved other gray nuclei that are straightforward to segment to benefit from them in the segmentation of Thalamus.

2. Proposed Method

Our proposed method consists of three major steps: 1) preprocessing; 2) shape vector extraction; and 3) final segmentation.

2.1 Preprocessing

Before we extract shape information, some preprocessing steps are required. As seen in Fig. 1, preprocessing steps are: 1) preprocessing of the image histogram; and 2) image alignment. Preprocessing is done to eliminate the effect of imaging equipment gain and

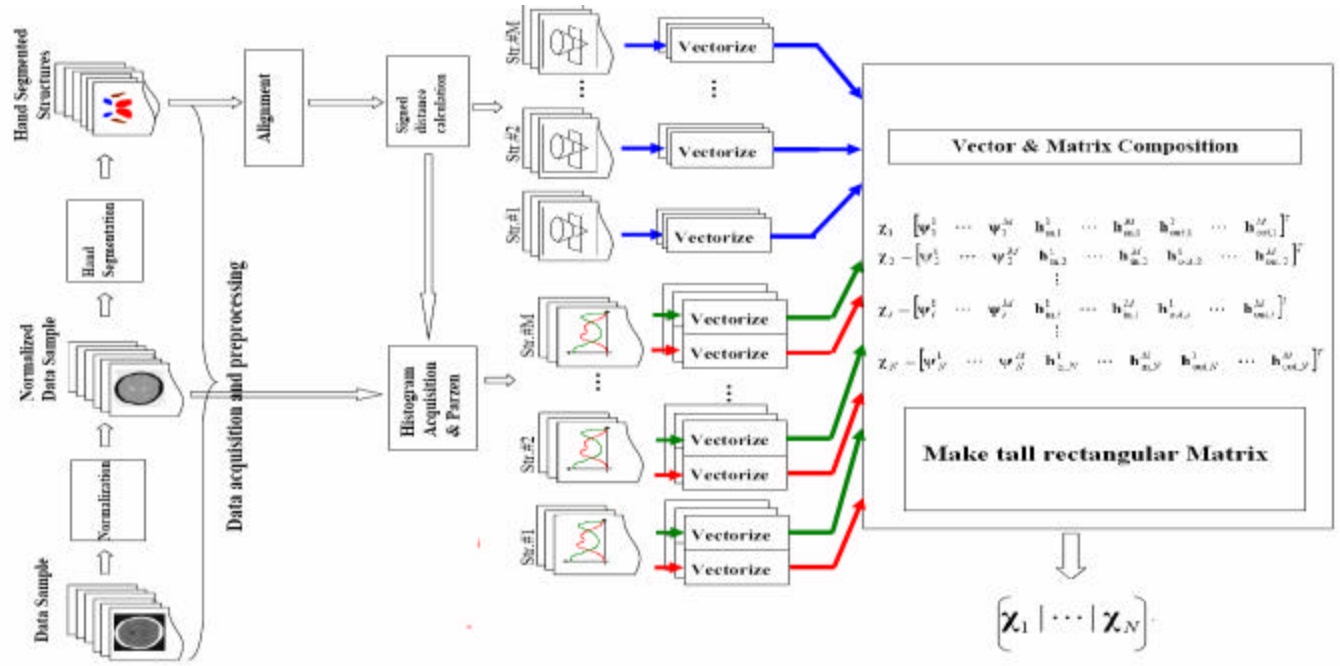

Fig. 1. Schematic of the proposed algorithm. Left part shows preprocessing stages while right part represents shape vector extraction. Str.#n denotes the n-th structure. Red graphs symbolize the interior and green graphs symbolize the exterior histogram. *Vectorize* blocks convert matrices to vectors.

other factors. Data alignment is done to extract real shape variation due to the anatomical changes and not those caused by misalignment.

We first normalize brain images to predetermined mean and standard deviation. Then, we ask an expert to segment the desired structures.

To align data samples to eliminate pose parameters effects, we use the method proposed by Tsai et al [10]. This approach possesses the following features: 1) it jointly aligns different shapes within a particular shape class; and 2) it performs alignment for all shape classes simultaneously.

Assume there are M segmented structures in the image which we would like to align to their corresponding structures. We encode each structure as a binary vector using 1 to indicate inside of the structure and 0 its outside. Therefore, we have vectors $?_i = [n_i^1 | n_i^2 | \cdots | n_i^m | \cdots | n_i^M]^T$ in which i indicates the number of the sample in the dataset ($1 \le i \le N$) and m denotes the number of the structure in the image. We find N vectors containing pose parameters. In 2D, the pose vectors are shown as $\mathbf{p} = [t_x \; t_y \; s \; q]^T$ in which t_x, t_y are the x and y translations and s, q are the scale and rotation parameters, respectively. Transformed binary vector are:

$$\hat{n}_i^m(\hat{x},\hat{y}) = n_i^m(x,y) \qquad (1)$$

$$\begin{bmatrix}\hat{x}\\ \hat{y}\\ 1\end{bmatrix} = T[\mathbf{p}]\begin{bmatrix}x\\ y\\ 1\end{bmatrix} = \underbrace{\begin{bmatrix}1 & 0 & t_x\\ 0 & 1 & t_y\\ 0 & 0 & 1\end{bmatrix}}_{M(t_x,t_y)} \times \underbrace{\begin{bmatrix}s & 0 & 0\\ 0 & s & 0\\ 0 & 0 & 1\end{bmatrix}}_{S(s)} \times \cdots$$

$$\underbrace{\begin{bmatrix}\cos(q) & -\sin(q) & 0\\ \sin(q) & \cos(q) & 0\\ 0 & 0 & 1\end{bmatrix}}_{R(q)} \times \begin{bmatrix}x\\ y\\ 1\end{bmatrix}$$

The transformation matrix $T[\mathbf{p}]$ is the product of three matrices: $M(t_x,t_y)$ to translate, $S(s)$ to scale, and $R(q)$ to rotate the image.

To consider differences between all of the structures and all of data samples, we use the following cost function [10]:

$$E_{align} = \sum_{i=1}^{N}\sum_{\substack{j=1\\ i\neq j}}^{N}\left\{\sum_{m=1}^{M}\frac{\iint_\Omega (\hat{v}_i^m - \hat{v}_j^m)^2 dA}{\iint_\Omega (\hat{v}_i^m + \hat{v}_j^m)^2 dA}\right\} \qquad (2)$$

where Ω denotes the images domain. As stated in [6], the normalization term in the denominator of (2) prevents shrinking of the structures. We employ the gradient descend method to optimize the above cost function.

2.2 Shape vector extraction

Given aligned binary shapes vectors, we construct shape parameters. First, we calculate signed distance function from binary segmented images [14]. Then, we extract gray level histogram of the desired structures. We define two kinds of histograms for each structure: 1) the interior histogram for the pixels inside the structure; and 2) the exterior histogram for pixels outside the desired structure. Interior histogram is described:

$$h_{in}(u) = \frac{1}{A_R}\iint_{\Omega} K(u - I(\mathbf{x}))H(-y(\mathbf{x}))dA, \qquad A_R = \iint_{\Omega} H(-y(\mathbf{x}))dA \tag{3}$$

where K, $H(\cdot)$, and $y(\mathbf{x})$ are the Gaussian kernel, used in the Parzen estimator, and the Heaviside and signed distance functions, respectively. Same as the conventional level set, negative numbers are used for the inside of the desired structure.

Owning to the fact that assuming one Gaussian distribution for all of the exterior pixels is not a reasonable assumption, we define the following focus region so that the points farther from the boundary have smaller effects.

$$h_{out}(u) = \frac{1}{A_{R^c}}\iint_{\Omega} K(u - I(\mathbf{x}))\cdot e^{\frac{-y^2(\mathbf{x})}{a}}\cdot H(y(\mathbf{x}))dA \qquad A_{R^c} = \iint_{\Omega} e^{\frac{-y^2(\mathbf{x})}{a}}\cdot H(y(\mathbf{x}))dA \tag{4}$$

where a determines the effective focus.

Assuming we have N data samples and each one contains M structures, we have a signed distance function and two histograms for each of the M structures. Using the results, we construct the following vectors.

$$\mathbf{?}_i = \begin{bmatrix}\mathbf{?}_i^1 & \cdots & \mathbf{?}_i^M & \mathbf{h}_{\text{in},i}^1 & \cdots & \mathbf{h}_{\text{in},i}^M & \mathbf{h}_{\text{out},i}^1 & \cdots & \mathbf{h}_{\text{out},i}^M\end{bmatrix}^T,\ 1 \le i \le N$$
$$\mathbf{?}_i^m = \begin{bmatrix}y_{11}^m & y_{12}^m & \cdots & y_{pq}^m & \cdots & y_{PQ}^m\end{bmatrix},$$
$$\mathbf{h}_{\text{in}}^m = [h_1^m \quad h_2^m \quad \cdots \quad h_{l_1}^m], \qquad \mathbf{h}_{\text{out}}^m = [h_1^m \quad h_2^m \quad \cdots \quad h_{l_2}^m]. \tag{5}$$

where l_1 and l_2 are the numbers of bins in the interior and exterior histograms and P and Q are the number of pixels in the x and y directions, respectively. $\mathbf{?}_i^m$ is the signed distance map for the m-th structure in the i-th data sample and $\mathbf{h}_{in/out,i}^m$ contains the histogram values for the interior and exterior of the m-th structure in the i-th data sample. Given a tall rectangular shape vector for each data sample, we define the following matrix.

$$\mathbf{X} = [\mathbf{?}_1 \quad \cdots \quad \mathbf{?}_i \quad \cdots \quad \mathbf{?}_N] \tag{6}$$

We subtract mean vector ($\bar{\mathbf{?}}$), which is averaged on all available shape vectors, to obtain normalized data samples ($\tilde{\mathbf{X}}$). Due to the fact that there is a very large number of rows in $\tilde{\mathbf{X}}$, we use its transpose for singular value decomposition (SVD).

$$\frac{1}{N}\tilde{\mathbf{X}}^T\tilde{\mathbf{X}} = \mathbf{Y}\times\mathbf{S}\times\mathbf{Y}^T \tag{7}$$

where $\mathbf{Y}$ contains the eigenvectors of $\frac{1}{N}\tilde{\mathbf{X}}^T\tilde{\mathbf{X}}$ and $\mathbf{S}$ is a diagonal matrix with the corresponding eigenvalues. It can be shown that if $\mathbf{y}$ is an eigenvector of $\frac{1}{N}\tilde{\mathbf{X}}^T\tilde{\mathbf{X}}$, $\mathbf{u} = \tilde{\mathbf{X}}\times\mathbf{y}$ is the corresponding eigenvector of $\frac{1}{N}\tilde{\mathbf{X}}\tilde{\mathbf{X}}^T$.

Choose t most significant modes to represent the data, we represent the shape vector as:

$$\mathbf{?} = \bar{\mathbf{?}} + \hat{\mathbf{U}}\times\hat{\mathbf{S}}\times\mathbf{b}$$
$$\bar{\mathbf{?}} = \begin{bmatrix}\bar{\mathbf{?}}^1 & \cdots & \bar{\mathbf{?}}^M & \bar{\mathbf{h}}_{\text{in}}^1 & \cdots & \bar{\mathbf{h}}_{\text{in}}^M & \bar{\mathbf{h}}_{\text{out}}^1 & \cdots & \bar{\mathbf{h}}_{\text{out}}^M\end{bmatrix}^T \tag{8}$$

where $\hat{\mathbf{U}}$ is a rectangular matrix containing t selected eigenvectors and $\hat{\mathbf{S}}$ is a diagonal matrix with the corresponding eigenvalues.

2.3 Histogram-based segmentation model

Because the aforementioned formulas do not accommodate changes caused by the pose parameters, we embed pose parameters with (8). To this end, we use the strategy which we applied for image alignment:

$$\bar{y}^m(x,y) = \bar{y}^m(\hat{x},\hat{y}) + \hat{\mathbf{U}}^m\times\hat{\mathbf{S}}\times\mathbf{b}, \quad 1 \le m \le M$$
$$\begin{bmatrix}\hat{x} & \hat{y} & 1\end{bmatrix}^T = T[\mathbf{p}]\begin{bmatrix}x & y & 1\end{bmatrix}^T \tag{9}$$

where $T[\mathbf{p}]$ is defined in (1), $\hat{\mathbf{U}}^m$ is a rectangular matrix with the eigenvectors of the m-th structure's *signed distance function*, and $\bar{y}^m(x,y)$ is the mean vector rearranged into rectangular shape.

For accurate segmentation, we need to define a cost function to be optimized. To this end, we compare the histogram gathered during the training process to the calculated histogram obtained from the target image. We then consider the correlations between the structures shape and exterior and interior histograms. To compare two histograms, we use Bhattacharyya coefficient, a popular measure in tracking purpose [15].

Given $h(u)$ and $\hat{h}(u)$, distributions of the gray levels for a specific region of the estimated and target images, respectively, Bhattacharyya coefficient is defined.

$$r(h,h^*) = \int\sqrt{h(u)\hat{h}(u)}du \tag{10}$$

where u is index of histogram bins. Based on the above definition, we specify distance between histograms as:

$$d = \sqrt{1 - r(h,\hat{h})} \tag{11}$$

To simplify the calculations, we use squared distance and define the following cost function.

$$E_{\text{HistMatch}} = -\sum_{m=1}^{M} r(h_{\text{in}}^m,\hat{h}_{\text{in}}^m) - \sum_{m=1}^{M} r(h_{\text{out}}^m,\hat{h}_{\text{out}}^m) \tag{12}$$

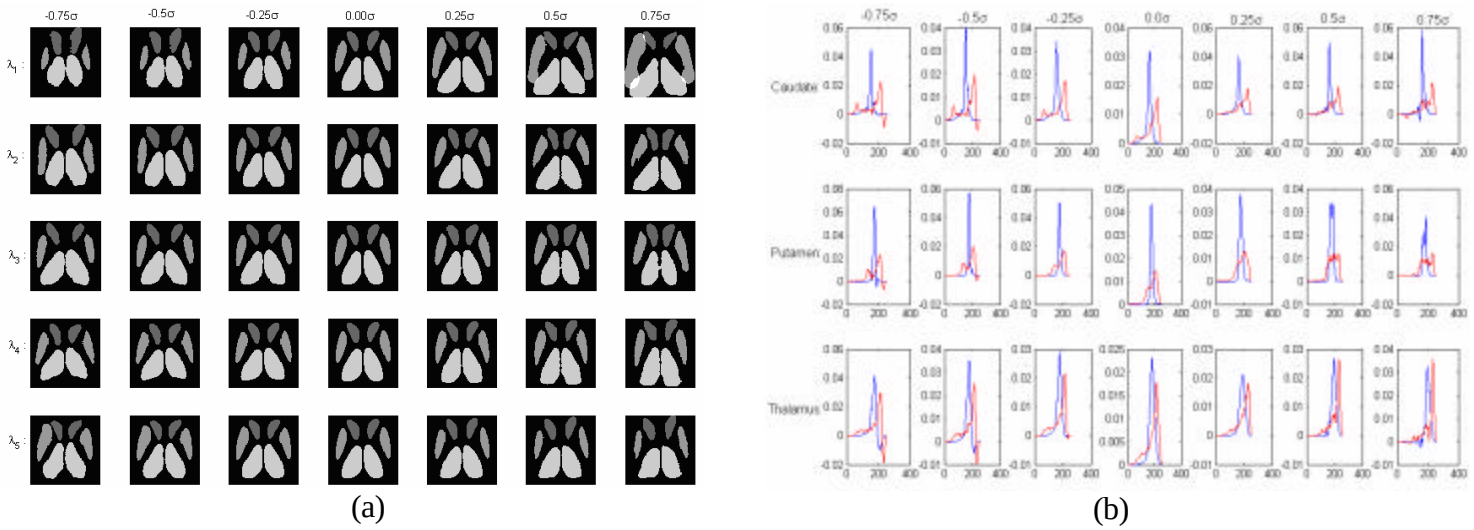

(a) (b)

Fig. 2. (a) The effects of the first five eigenvalues on the structures shapes are shows. The overlaps are due to the large values of the biggest eigenvalue. (b) The effects of the biggest eigenvalue on the interior and exterior histograms of the three structures are shown. Blue lines denote interior histogram and red lines represent exterior histogram. For this figure, we assumed $s=2$ for the Gaussian Kernel in the Parzen estimator and $a=0.05$ for the focus function.

In order to optimize the above functions using either the steepest descend or the conjugate gradient, we need its derivation. Gradient of $E_{\text{HistMatch}}$ in respect to $\mathbf{b}_t$ and $\mathbf{p}$ are:

$$\begin{aligned}\nabla_{\mathbf{p}} E_{\text{HistMatch}} &= -\sum_{m=1}^{M} \nabla_{\mathbf{p}} r(h_{\text{in}}^m, \hat{h}_{\text{in}}^m) - \sum_{m=1}^{M} \nabla_{\mathbf{p}} r(h_{\text{out}}^m, \hat{h}_{\text{out}}^m), \\ \nabla_{\mathbf{b}} E_{\text{HistMatch}} &= -\sum_{m=1}^{M} \nabla_{\mathbf{b}} r(h_{\text{in}}^m, \hat{h}_{\text{in}}^m) - \sum_{m=1}^{M} \nabla_{\mathbf{b}} r(h_{\text{out}}^m, \hat{h}_{\text{out}}^m).\end{aligned} \tag{13}$$

The k-th elements of the gradient vector $\nabla_{\mathbf{p}} r$ and $\nabla_{\mathbf{b}} r$ are given by:

$$\nabla_{\mathbf{a}} r(h_{\text{in}}^m, \hat{h}_{\text{in}}^m) = -\frac{1}{2A^{R_m}} \oint_{\tilde{C}_m} \sqrt{\frac{\hat{h}_{\text{in}}^m}{h_{\text{in}}^m}} \cdot \nabla_{\mathbf{a}} y \cdot K(u - I(s)) ds.du \tag{14}$$

$$\begin{aligned}\nabla_{\mathbf{a}} r(h_{\text{out}}^m, \hat{h}_{\text{out}}^m) = &\frac{1}{2A^{R_m^c}} \oint_{\tilde{C}_m} \sqrt{\frac{\hat{h}_{\text{in}}^m}{h_{\text{in}}^m}} \cdot \nabla_{\mathbf{a}} y \cdot e^{\frac{-y^2(s)}{a}} \cdot K(u - I(s)) ds.du \\ &- \frac{1}{A^{R_m^c}} \iint_{\Omega} \sqrt{\frac{\hat{h}_{\text{in}}^m}{h_{\text{in}}^m}} \cdot \nabla_{\mathbf{a}} y \cdot y(\mathbf{x}) \cdot \frac{y(\mathbf{x})}{a} \cdot e^{\frac{-y^2(\mathbf{x})}{a}} \cdot K(u - I(\mathbf{x})) H(y(\mathbf{x})) dx.du\end{aligned} \tag{15}$$

where $\mathbf{a} = \{\mathbf{b}, \mathbf{p}\}$ and $\nabla_{\mathbf{b}} y$ and $\nabla_{\mathbf{p}} y$ are:

$$\begin{aligned}&\nabla_{\mathbf{b}^k} y = \mathbf{u}^k, \qquad 1 \le k \le t, \\ &\nabla_{\mathbf{p}^l} y = \begin{bmatrix} \frac{\partial y(\hat{x},\hat{y})}{\partial \hat{x}} & \frac{\partial y(\hat{x},\hat{y})}{\partial \hat{y}} & 0 \end{bmatrix} \frac{\partial T[\mathbf{p}^k]}{\partial \mathbf{p}^k} \begin{bmatrix} x \\ y \\ 1 \end{bmatrix}, \quad 1 \le l \le 4 \\ &\frac{\partial T[\mathbf{p}^1]}{\partial \mathbf{p}^1} = \frac{\partial T[\mathbf{p}]}{\partial t_x} = \frac{\partial M(t_x, t_y)}{\partial t_x} S(s) R(q), \\ &\frac{\partial T[\mathbf{p}^1]}{\partial \mathbf{p}^2} = \frac{\partial T[\mathbf{p}]}{\partial t_y} = \frac{\partial M(t_x, t_y)}{\partial t_y} S(s) R(q), \\ &\frac{\partial T[\mathbf{p}^1]}{\partial \mathbf{p}^3} = \frac{\partial T[\mathbf{p}]}{\partial s} = M(t_x, t_y) \frac{\partial S(s)}{\partial s} R(q), \\ &\frac{\partial T[\mathbf{p}^1]}{\partial \mathbf{p}^4} = \frac{\partial T[\mathbf{p}]}{\partial q} = M(t_x, t_y) S(s) \frac{\partial R(q)}{\partial q}.\end{aligned} \tag{16}$$

Using the steepest descend method, update equations for the parameters are:

$$\begin{aligned}\mathbf{b}^+ &= \mathbf{b}^- - \Delta t_{\mathbf{b}} \nabla_{\mathbf{b}} E_{\text{HistMatch}}, \\ \mathbf{p}^+ &= \mathbf{p}^- - \Delta t_{\mathbf{p}} \nabla_{\mathbf{p}} E_{\text{HistMatch}}.\end{aligned} \tag{17}$$

3 Experimental Results

We tested our method on real T1 magnetic resonance images from the Internet Brain Segmentation Repository (IBSR) [12]. Each volume contains 128 slices in the

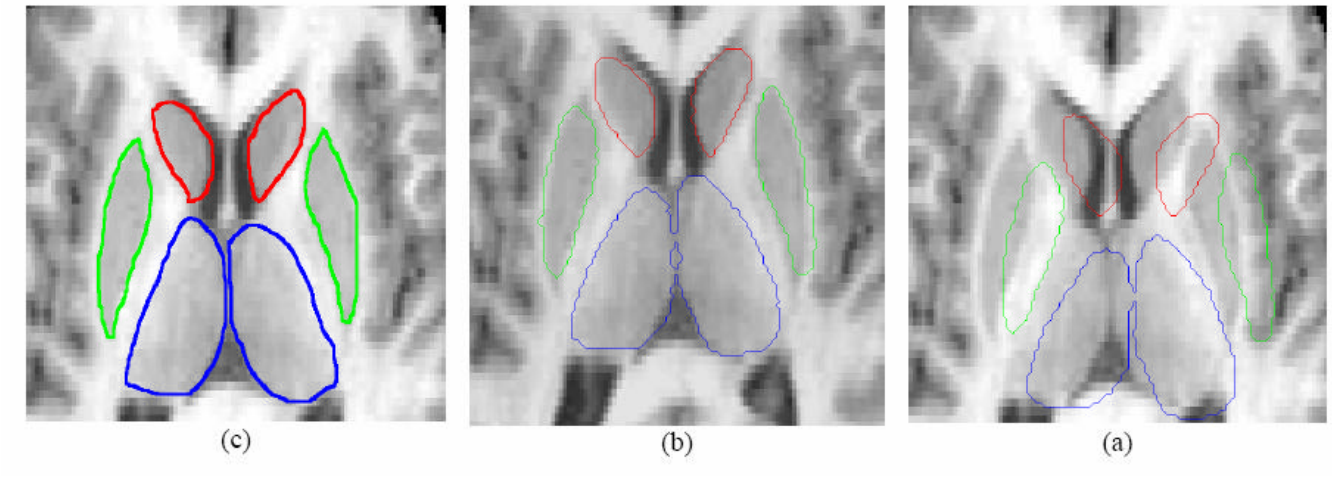

Fig. 3. (a) Coarse initialization of the contours. (b) Final results. (c) Manually segmented results.

Table 1. Results of 3 cases. White blocks show the initialization results and gray blocks show the final results. The values outside the parantesis are the Hausdorf distances and the values inside the parantesis are the overlapping measure.

	Left Caudate	Right Caudate	Left Putamen	Right Putamen	Left Thalamus	Right Thalamus
Case1	4.0(47%)	5.0(20%)	4.42(26%)	5.13(22%)	4.89(61%)	5.2(64%)
	1.24(83%)	0.78(92%)	0.63(94%)	1.04(88%)	0.81(93%)	1.18(96%)
Case2	3.82(47%)	2.92(64%)	3.99(42%)	4.1(32%)	4.45(64%)	3.97(64%)
	1.02(80%)	0.8(88%)	0.81(82%)	1.05(81%)	1.19(88%)	1.1(80%)
Case3	1.06(89%)	1.23(86%)	2.6(65%)	2.07(68%)	2.67(84%)	2.28(83%)
	0.53(95%)	0.59(96%)	1.19(84%)	1.02(82%)	1.12(96%)	0.77(93%)

coronal plane. The slice thickness is 1mm and the image matrix size is 256x256. The distance between each two pixels is 0.93mm. Using the nearest neighbor method, the coronal slices were interpolated to construct the axial images.

In the preprocessing step, we chose 31 axial images to derive averages for the mean and standard deviation. For the exterior focus region, we set a=0.05 in (4). To minimize the algorithm execution time, we neglected points with focus weights less than 0.1. We used 256 bins histograms for the interior and exterior regions (l_1=l_2=256).

Considering the image size (256x256), the number of structures (M=3), and the histogram bins, the dimension of shape vectors are about 198,144. We chose 20 most important eigenvectors (t=20) as their corresponding eigenvalues contain 92% of the sum of all eigenvalues. We constrained elements of $\mathbf{b}$ to $0.4s$ to avoid conflict (see the upper most right in Fig. 2a). Moreover, we set the negative values of the histograms to zero (see Fig. 2b).

We evaluated our method using three slices of three different patients, not used in the training phase. As seen in Fig. 3, segmentation was started from a rough initialization defined by the atlas. Although initial contours may seem accurate near Caudate, they are not accurate for Thalamus and Putamen. Taking advantage of the reasonable initial contour for the Caudate in addition to *a priori* information about the interior and exterior histograms of the desired structures and their shapes, our model generated accurate results. Because we based our method on both of the gray level information and the shape knowledge, it was neither distracted by the gray level of cortex pixels (Putamen) nor their heterogeneity (Thalamus).

To evaluate the algorithm's performance quantitatively, we used two measures: 1) Hausdorf distance of the boundaries; and 2) the common area between two regions:

$$H(A,B)=\max(h(A,B),h(B,A)),\quad h(A,B)=\frac{1}{N_A}\sum_{a\in A}\min_{b\in B}\|a-b\| \tag{18}$$

$$Similarity=\frac{Area(A)\cap Area(B)}{Area(B)} \tag{19}$$

where A and B are sets containing the boundary points of the automatically segmented and manually segmented regions, respectively. Table 1 shows the final result of our algorithm.

4 Conclusion

We have proposed a novel method to most efficiently use both of the shape priori and histogram information of the desired structure in its segmentation. Our method shares common features with the Active Appearance Model (AAM) proposed by Cootes et al [13] in that both methods use shape priori and gray level information of the desired structures. However, our approach has advantages such as robustness against landmarks inaccuracies as it does not use them; it uses the signed distance function instead. Our method is also related to the Tsai et al method [6], which uses the signed distance function to exploit the shape priori. However, we tested our method on a challenging structure (Thalamus), which they did not. Our histogram-based method is related to that of [7]. However, we only considered the pixels in a focus region instead of considering all of the exterior pixels.

The complicated equations used in the gradient descend method can be avoided if a numerical method is employed. We tested the BFGS Quasi-Newton numerical method with a mixed quadratic and cubic line search procedure, which worked well for our application.

References

1. S. Osher and J. Sethian, "Fronts propagating with curvature-dependent speed: Algorithms based on Hamiltons–Jacobi formulations," *J. Comput. Phys.*, vol. 79, no. 1, pp. 12–49, 1998.
2. W. Kass and D. Terzopolous, "Snakes: Active contour models," *Int. J. Comput. Vision*, vol. 1, no. 4, pp. 321–331, 1988.
3. T. F. Cootes, C. J. Taylor, D. H. Cooper, and J. Graham, "Active shape models: Their training and applications," *Comput. Vision Image Understanding*, vol. 61, no. 1, pp. 38–59, 1995.
4. Jasjit S. Suri, Kecheng Liu, Sameer Singh, Swamy N. Laxminarayan, Xiaolan Zeng, and Laura Reden, "Shape Recovery Algorithms Using Level Sets in 2-D/3-D Medical Imagery: A State-of-the-Art Review," *IEEE Trans. on Info. Tech. in Biomedicine*, vol. 6, no. 1, pp. 8-28, 2002.
5. M. E. Leventon,W. Grimson, L. Eric, and O. Faugeras, "Statistical shape influence in geodesic active contours," *Proc. Comput. Vision Pattern Recognition (CVPR)*, vol. 1, pp. 316–323, 2000.
6. A. Tsai, W. Wells, C. Tempany, E. Grimson, A. Willsky, "Mutual information in coupled multi-shape model for medical image segmentation," *Med. Imag. Analys.*, vol. 8, pp. 429–445, 2004.
7. J. Yang, L. H. Staib, J. S. Duncan, "Neighbor-Constrained Segmentation With Level Set Based 3-D Deformable Models," *IEEE Trans. on Med. Imaging.*, vol. 23, no. 8, pp. 940-948, 2004.
8. V. Barra, J. -Y. Boire, "Automatic Segmentation of Subcortical Brain Structures in MR Images Using Information Fusion," *IEEE Transaction on Medical Imaging*, vol. 20, no. 7, pp. 549-558, 2001.
9. L. Amini, H. Soltanian-Zadeh, C. Lucas, M. Gity, "Automatic Segmentation of Thalamus From Brain MRI Integrating Fuzzy Clustering and Dynamic Contours," *IEEE Trans. on Biomed. Eng.*, vol. 51, no.5, pp. 800-811, 2004.
10. A. Tsai, A. Yezzi, W. Wells, C. Tempany, D. Tucker, A. Fan, W. E. Grimson, A. Willsky, "A Shape-Based Approach to the Segmentation of Medical Imagery Using Level Sets," *IEEE Trans. on Med. Imag.*, vol.22, no.2, pp.137-154, 2003.
11. T. F. Chan, L. A. Vese, "Active Contours without Edges," *IEEE Trans. on Image Process.*, vol.10, no.2, pp.266-277, 2001.
12. http://www.cma.mgh.harvard.edu/ibsr/
13. T.F. Cootes, C.J. Taylor, "Statistical Models of Appearance for Computer Vision," *Technical Report, Imaging Science and Biomedical Engineering, Univ. of Manchester*, 2001.
14. S. Osher, N. Paragios, "Geometric Level Set Method in Imaging, Vision, and Graphics," Springer- Verlag NY., pp.7-12, 2003.
15. Katja Nummiaroa, Esther Koller-Meierb, Luc Van Goola, "An adaptive color-based particle filter," *Image and Vision Comp.*, vol. 21, pp. 99–110, 2003